Available online at www.tjnsa.com
J. Nonlinear Sci. Appl. 9 (2016), 1609–1618
Research Article

A topological analysis on patches of optical flow

Shengxiang Xia

College of Science, Shandong Jianzhu University, Jinan 250101 P.R. China.

Communicated by R. Saadati

Abstract

The research of optical flow is vitally important topic in computer vision. In this paper we research a topological analysis of space of optical flow locally. We use the methods of computing topology to the spaces of 4×4 and 6×6 high contrast optical flow patches. We experimentally prove that in both cases there exist subspaces of the spaces of all high contrast optical flow patches that is topologically equivalent to a circle, which states that some results on the topological analysis of natural images and range images can be extended to the scope of image motion.

Keywords: Optical flow, high contrast patches, persistent homology, plex barcodes, Klein bottle.
2010 MSC: 62H35, 65D18.

1. Introduction

Optical flow was defined by J. J. Gibson [10], it is the ostensible motion of brightness patterns viewed by the viewer, when a camera is moving relative to the objects being imaged. Hence, optical flow can provide very important information about the spatial arrangement of objects observed. Optical flow estimation is a basic study topic in computer vision, it involves with calculating the motion of pixels between consistent image frames. A large number of results about this topic have been obtained in recent years [4, 5, 11, 15]. Natural image statistics have attracted a large number of scholars to study and have gained fruitful results on them, but for statistics of optical flow, because of the difficulty of gaining data of optical flow, the optical flow statistics are comparatively unexplored. In recent years, some databases of optical flow are built sequentially, for example, S. Roth and M. J. Black created a database of natural scene motions by using of range images and camera motions [13]. The other two databases of optical flow are constructed respectively in the papers [4, 9]. H. Adams, A. Atanasov and G. Carlsson [1] used the nudged elastic band method to analyze the optical flow database. They discovered a new topological property of an optical flow

Email address: xias@sdjzu.edu.cn (Shengxiang Xia)

Received 2015-09-30

data set of 3×3 patches. As the optical flow database [13] is constructed from the Brown range image database, spaces of 4×4 and 6×6 optical flow patches perhaps have same topological characteristics as small range image patches. In fact, such similar topological properties between 3×3, 5×5 and 7×7 range image patches and optical flow patches have been discovered in the papers [1, 2, 16, 17].

The spaces of 4×4 and 6×6 range image patches were studied in [18]. In this paper, we apply the methods of the paper [7] to high contrast regions of optical flow and discuss the topological structure of spaces of 4×4 and 6×6 optical flow patches. We experimentally show that there exist two dimensional subspaces in each of spaces of 4×4 and 6×6 optical flow patches, whose homology is that of a circle. Furthermore, we detect that there exist subspaces of 4×4 and 6×6 patches of optical flow, they probably have Klein bottle feature. Thus there exist similar topological properties between 4×4 and 6×6 range image patches and optical flow patches.

2. Persistent homology

For a finite point set $\mathbb{X}$ sampled from a fundamental space $Y \subseteq \mathbb{R}^m$, along with a parameter ϵ, we could build a simplicial complex with it, called the Vietoris-Rips complex, represented by $\mathcal{R}_\epsilon$. The vertex set of the complex is $\mathbb{X}$ and a subset $\{x_0, x_1, ..., x_k\}$ will define a k-simplex in $\mathcal{R}_\epsilon$ if and only if $d(x_i, x_j) \leq \epsilon$ for all $0 \leq i, j \leq k$. A $\mathcal{R}_\epsilon$ complex can be computed at every value ϵ. It is obvious that $\mathcal{R}_0$ is a 0-complex and $\mathcal{R}_\infty$ is an $(\mid \mathbb{X} \mid -1)$-simplex.

In order to study the space Y by using a $\mathcal{R}_\epsilon$ complex, Edelsbrunner, Letscher and Zomorodian [8] introduced the concept of persistence, later, Carlsson and Zomorodian [19] elaborated it. If $\epsilon \leq \epsilon'$, a natural inclusion of simplicial complexes $\mathcal{R}_\epsilon \hookrightarrow \mathcal{R}_{\epsilon'}$ is obvious and therefore $H_k(\mathcal{R}_\epsilon) \longrightarrow H_k(\mathcal{R}_{\epsilon'})$ for any k.

For persistence vector spaces, they can be described by an invariant called a barcode which is just a finite collection of intervals, it was shown that any two persistence vector spaces having same barcodes are isomorphic. Long intervals in barcodes denote a real topological structure of an underlying space, but small intervals are thought to be inadequate sampling.

Because VR complexes could yield simplex in dimensions much higher than that of the fundamental space, in a real application we utilize the witness complex introduced in [14].

For a point cloud Q, a landmark subset L and a parameter $r \in \mathbb{N}$, if $r = 0$, let $m(q) = 0$ for all $q \in Q$. If $r > 0$, let $m(q)$ be the distance q to the r-th closest landmark point. The lazy witness complex $LW_r(Q, L, \epsilon)$ is defined as follows:

(i) the vertex set is L;

(ii) for vertices a and b, edge [ab] is in $LW_r(Q, L, \epsilon)$ if there is a witness point $q \in Q$ such that

$$\max\{d(a, q), d(b, q)\} \leq \epsilon + m(q);$$

(iii) a higher dimensional simplex is in $LW_r(Q, L, \epsilon)$ if all of its edges are.

The lazy witness complex depends upon a parameter $r \in \{0, 1, 2\}$ which we select $r = 1$. De Silva and Carlsson in [14] discover $r = 0$ to be generally less effective and $r = 2$ has the disadvantage of connecting every landmark point to at least one other at $R = 0$. Please refer to the papers [3, 6, 14, 19] for more details about lazy witness complexes and persistent homology.

We consider a point cloud set and a sequence of VR complexes as illustrated in Figure 1 (a), (b), (c), and (d). This point cloud is a sampling of points on a planar circle. Can this be deduced? We observe that there exists an inclusion of the current complex in the next complex (from (a) to (d)), as the current one corresponds to a smaller parameter value than the next one. From the Figure 1, we note that there are two small holes in Figure 1 (b), while one small hole has been filled in, a new large hole has been introduced in Figure 1 (c). As increasing, the two small holes vanish, because they are filled in as indicated in Figure 1 (d). Therefore, we conclude that the image consists exactly of the larger hole, which is what we regard as the correct answer in this case.

The bottom of Figure 1 shows an example of barcode denotations of the homology of the sampling of points. Form Figure 1 we survey that there exist one long line in dimension 0, one in dimension 1 and

no line in dimension 2 (ϵ varying from 3.82 to 7) which reflects the fact that a circle has one connected component and one hole in dimension one.

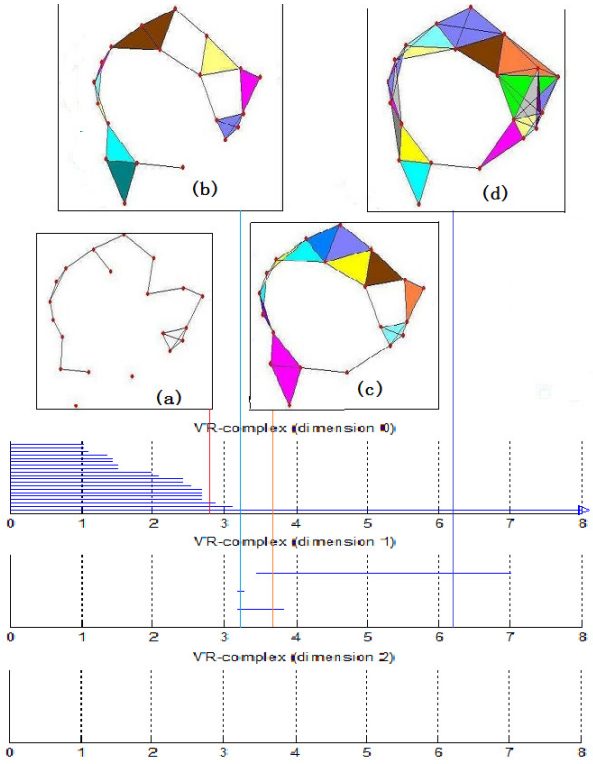

Figure 1: The barcodes for the sequence complexes VR_ϵ, $0 \leq \epsilon \leq 7$.

3. Constructing spaces of small optical flow patches

We gather data sets of high contrast 4×4 and 6×6 optical flow patches from the Roth and Black optical flow database [13], the database is available at http://www.visinf.tu-darmstadt.de/vi_research/vi_datasets/vi_ flowstats.en.jsp. There are two samples of it in Figure 2.

We randomly choose data sets of 4×4 and 6×6 high contrast patches from the optical flow database. The main spaces M_4 and M_6 are sets of 4×4 and 6×6 high contrast patches produced by the follows six steps (similar to [2, 7, 12]). M_4 and M_6 posses about 220000 points.

Step 1. For each flow field sequence in the database, we utilize the second optical flow frame of a sequence and randomly pick 1500 $n \times n$ $(n = 4, 6)$ patches for it. One 4×4 patch is arranged as

$$\begin{pmatrix} (u_1, v_1) & (u_5, v_5) & (u_9, v_9) & (u_{13}, v_{13}) \\ (u_2, v_2) & (u_6, v_6) & (u_{10}, v_{10}) & (u_{14}, v_{14}) \\ (u_3, v_3) & (u_7, v_7) & (u_{11}, v_{11}) & (u_{15}, v_{15}) \\ (u_4, v_4) & (u_8, v_8) & (u_{12}, v_{12}) & (u_{16}, v_{16}) \end{pmatrix}$$

and one 6×6 patch is arranged as

$$\begin{pmatrix} (u_1, v_1) & (u_7, v_7) & (u_{13}, v_{13}) & (u_{19}, v_{19}) & (u_{25}, v_{25}) & (u_{31}, v_{31}) \\ (u_2, v_2) & (u_8, v_8) & (u_{14}, v_{14}) & (u_{20}, v_{20}) & (u_{26}, v_{26}) & (u_{32}, v_{32}) \\ (u_3, v_3) & (u_9, v_9) & (u_{15}, v_{15}) & (u_{21}, v_{21}) & (u_{27}, v_{27}) & (u_{32}, v_{32}) \\ (u_4, v_4) & (u_{10}, v_{10}) & (u_{16}, v_{16}) & (u_{22}, v_{22}) & (u_{28}, v_{28}) & (u_{34}, v_{34}) \\ (u_5, v_5) & (u_{11}, v_{11}) & (u_{17}, v_{17}) & (u_{23}, v_{23}) & (u_{29}, v_{29}) & (u_{35}, v_{35}) \\ (u_6, v_6) & (u_{12}, v_{12}) & (u_{18}, v_{18}) & (u_{24}, v_{24}) & (u_{30}, v_{30}) & (u_{36}, v_{36}) \end{pmatrix},$$

where u indicates optical flow in the horizontal direction and v indicates the vertical direction. Consider each 4×4 patch as a vector $\mathbf{x} = (u_1, ..., u_{16}, v_1, ..., v_{16}) \in \mathbb{R}^{32}$ and each 6×6 patch as a vector $\mathbf{x} = (u_1, ..., u_{36}, v_1, ..., v_{36}) \in \mathbb{R}^{72}$.

Step 2. We calculate the D-norm $\| \mathbf{x} \|_D$ for each vector $\mathbf{x}$, it is a measure of the contrast of a optical flow patch. Two pairs of coordinates (u_i, v_i) and (u_j, v_j) of $\mathbf{x}$ are adjacent, represented by $i \sim j$, if the corresponding pixels in the $n \times n$ patch are neighbors. We compute the D-norm for a vector $\mathbf{x}$ by using the formula: $\| \mathbf{x} \|_D = \sqrt{\sum_{i \sim j} \| (u_i, v_i) - (u_j, v_j) \|^2}$.

Step 3. We choose the patches which have a D-norm in the top 20% of each sequence as usually.

Step 4. For u components, subtract an average of u coordinates and for v components, subtract an average of v coordinates, this will produce a new 32-dimension vector and a new 72-dimension vector, respectively.

Step 5. We map the spaces into a unit sphere by dividing each vector with its Euclidean norm, that is not zero since the patches are high contrast. We do not transform to the DCT basis for convenience.

Step 6. For the convenience of calculations, we randomly choose 50,000 from above patches in the top 20% and these sets are subspaces of M_4 and M_6, represented as MS_4 and MS_6, respectively.

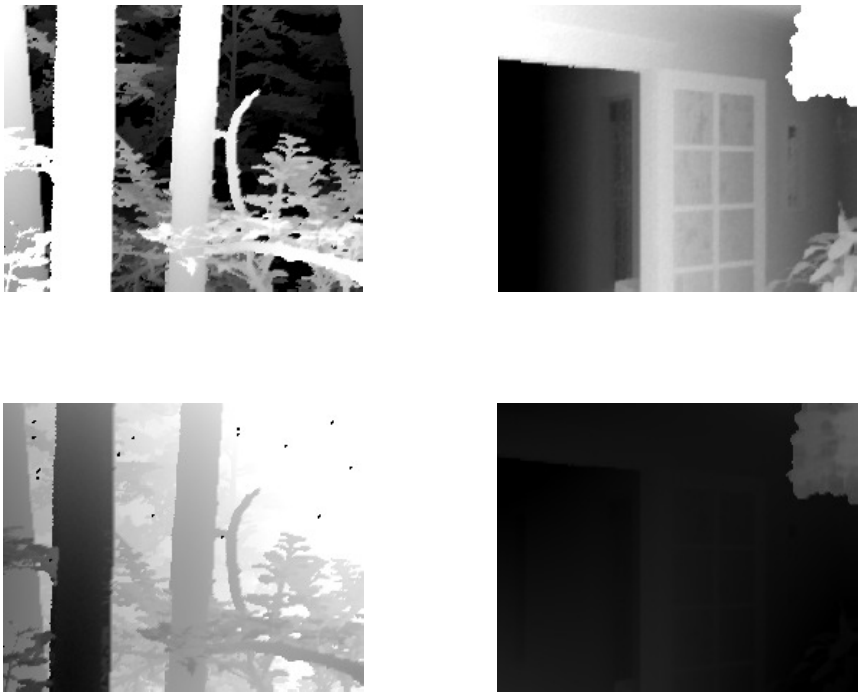

Figure 2: Two samples from the database. Horizontal motions are on the top and vertical motions are on the bottom.

4. Experimental results for $MS^m(k, p)$

The 3×3, 5×5 and 7×7 range image patches have core subsets with topological feature of a circle were shown by Xia in [16] and H. Adams and G. Carlsson in [2]. The spaces of 3×3 , 5×5 and 7×7 optical flow patches having core subsets with topology of a circle were shown in the papers [1, 17]. We will extend the result to 4×4 and 6×6 optical flow patches. The concept of core subsets is used to detect the

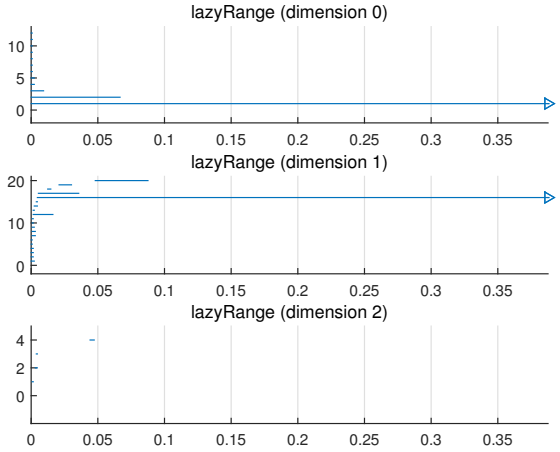

Figure 3: Barcodes for $MS^4(200, 30)$.

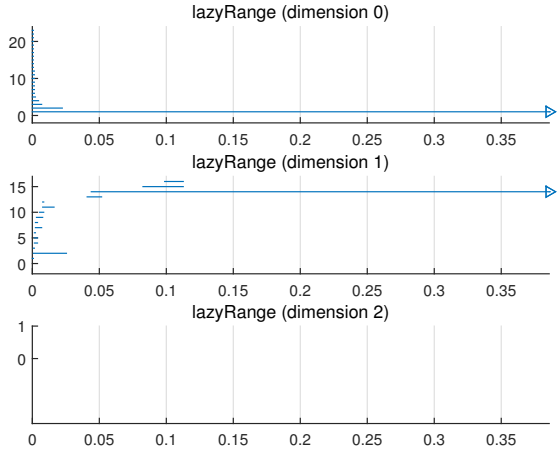

Figure 4: Barcodes for $MS^6(200, 30)$.

circle feature of MS_4 and MS_6. We estimate the local density of the space at a point x by its the nearest neighbor. For $x \in X$ and $k > 0$, set $\rho_k(x) =\mid x - x_k \mid$, where x_k is the k-th nearest neighbor of x. Larger k-values generate more global evaluations, while small k-values provide local density evaluates. For a given k, we order points of X by descending density, we choose the points denoted by $X(k, p)$ whose densities are in the top p percent.

We think about the core subsets $MS^4(200, 30)$ and $MS^6(200, 30)$ and calculate their barcodes, samples Betti barcode plots for them are shown in Figures 3 and 4 separately. There exist a long $Betti_0$ interval and a long $Betti_1$ interval in the plots, that is $\beta_0 = 1$, $\beta_1 = 1$, with the topology of a circle. We make three hundreds experiments on the core subsets $MS^4(100, 30)$, $MS^4(300, 30)$, $MS^6(100, 30)$ and $MS^6(300, 30)$, all the barcode plots have the homology of the circle and the results are stable.

5. A theoretic model for Klein bottle

The Klein bottle can be obtained by pasting a square as shown in Figure 5. In the process of identification, three circles are informed (Figure 6), represented by C_3.

To detect the topological features of subspaces of M_4 and M_6, we create another theoretical model for the Klein bottle. We think $n \times n$ optical flow patches as obtained by sampling smooth real-valued polynomials on the xy-plane at $n \times n$ grid points. We now consider the space $\mathcal{P}$, consisting of polynomials in form of $a_2(a_1x + b_1y)^2 + b_2(a_1x + b_1y)$, $(a_1, b_1) \in S^1$, $(a_2, b_2) \in S^1$, where S^1 is the unit circle.

We define the map $g : S^1 \times S^1 \longmapsto \mathcal{P}$ by $(a_1, b_1, a_2, b_2) \longmapsto a_2(a_1x+b_1y)^2+b_2(a_1x+b_1y)$ ([7]). Clearly, the map g is onto, but not one-one, this means that $(a_1, b_1, a_2, b_2) \sim (-a_1, -b_1, a_2, -b_2)$ is an equivalent relation. If (a_1, b_1, a_2, b_2) is denoted by $(\cos\alpha, \sin\alpha, \cos\beta, \sin\beta)$, both α and β vary in $[0, 2\pi]$, then the equivalent relation is $(\alpha, \beta) \sim (\pi+\alpha, 2\pi-\beta)$. The space $\mathcal{P}$= im(g) is homeomorphic to $S^1 \times S^1/(\alpha, \beta) \sim (\pi+\alpha, 2\pi-\beta)$, because no other identifications mapped by g.

The result of the map g acting on a square is shown in Figure 7. Each half is an indication of the Klein bottle, hence the image of g is homeomorphic to the Klein bottle and so is $\mathcal{P}$ ([7]).

The model C_3 is included in the space $\mathcal{P}$. The primary circle of C_3 is the subspace obtained by setting $(a_2, b_2) = (0, 1)$ and $(a_1, b_1) \in S^1$, however the other circles are gained by setting $a_1 = 1, b_1 = 0$ and $a_1 = 0, b_1 = 1$ respectively.

We define $h_4 : \mathcal{P} \longmapsto S^{31}$ by a composite of evaluating the polynomial at every point in the grid $G_4 = \{-3, -2, -1, 0, 1, 2, 3, 4\} \times \{-1, 0, 1, 2\}$ subtracting the mean and normalizing. We define $h_6 : \mathcal{P} \longmapsto S^{71}$ by a composite of evaluating polynomials at each point in the grid $G_6 = \{-5, -4, -3, -2, -1, 0, 1, 2, 3, 4, 5, 6\} \times \{-2, -1, 0, 1, 2, 3\}$ subtracting the mean and normalizing.

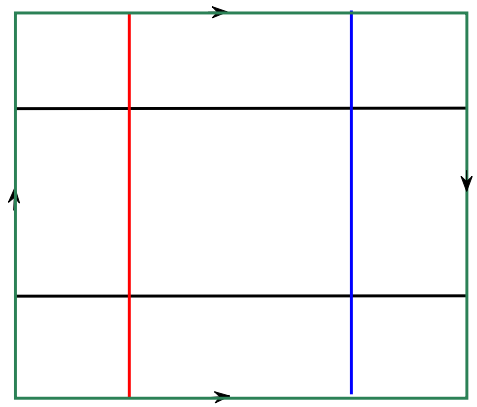

Figure 5: One denotation of Klein bottle.

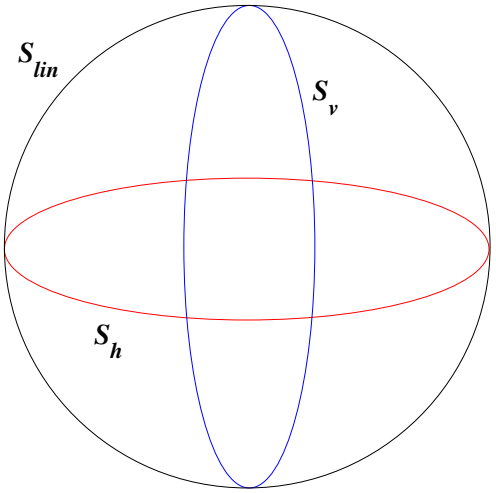

Figure 6: Three circle model.

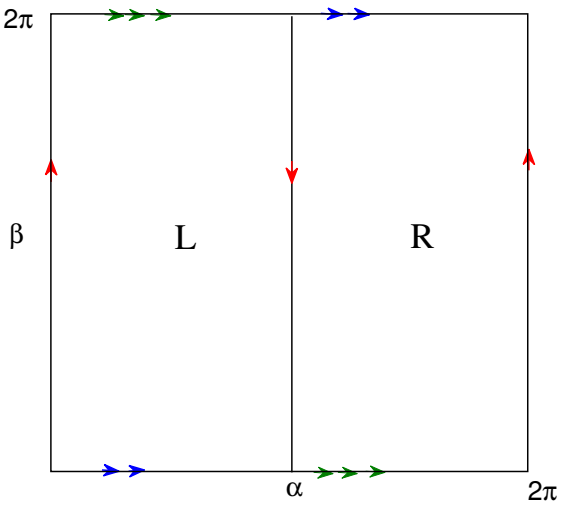

Figure 7: Klein bottle, the image of the map g.

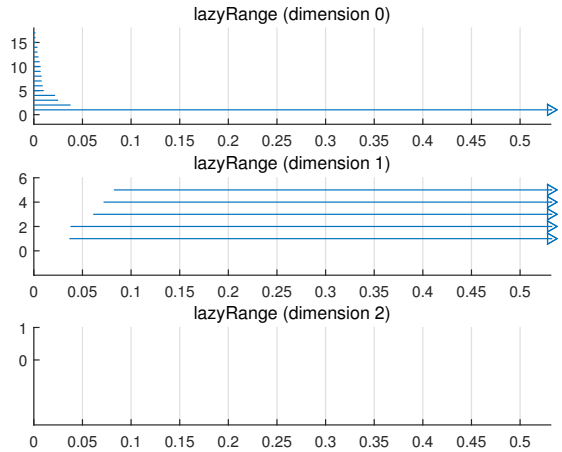

Figure 8: Barcodes for $C_3^4(400)$.

As the proof in [7], h_4 and h_6 are one-to-one. Since a compact space is homeomorphic to its image under continuous one-to-one mapping, hence the image $im(h_n \mid \mathcal{P})(n = 4, 6)$ is homeomorphic to the Klein bottle.

To embed the space C_3 into the unit sphere S^{31}, we randomly take 400 points $\{(x_1, y_1), ..., (x_{400}, y_{400})\}$ on S^1, then put $a_2 = 0, b_2 = 1$; $a_1 = 1, b_1 = 0$; $a_1 = 0, b_1 = 1$ respectively, we denote the set of all images of the 400 points under the map $h_4 \circ g$ as $C_3^4(400)$. Similarly, we have $C_3^6(400)$. Figures 8, 9 display the PLEX result for the spaces $C_3^4(400)$ and $C_3^6(400)$, they have the topology of C_3, i.e. $\beta_0 = 1, \beta_1 = 5$, thus we acquire an appropriate approach of C_3 in S^{31} and S^{71}, respectively.

In order to embed the Klein bottle into a unit sphere, firstly, we uniformly take 200 points $(\{x_1, ..., x_{200}\})$ on the unit circle, all possible tuples (x_i, x_j) form a point set on $S^1 \times S^1$. Next, we denote the images of the 40000 points under the mappings $h_4 \circ g$ and $h_6 \circ g$ as $K^4(200)$ and $K^6(200)$, respectively. Figure 10 gives the PLEX result for the spaces $K^4(200)$ with $\beta_0 = 1, \beta_1 = 2$ and $\beta_2 = 1$, which are the mod 2 Betti numbers of the Klein bottle. Hence, $K^4(200)$ is a proper approach of the Klein bottle in S^{31}. We have a similar result for the space $K^6(200)$ (Figure 11).

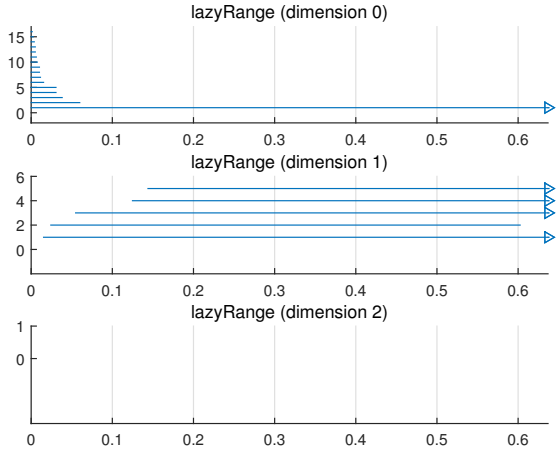

Figure 9: Barcodes for $C_3^6(400)$.

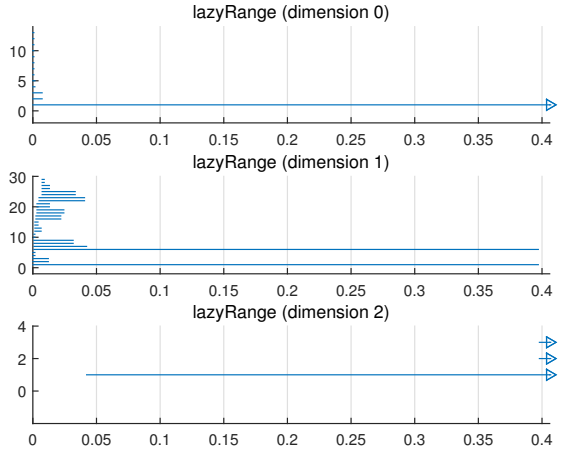

Figure 10: Barcodes for $K^4(200)$.

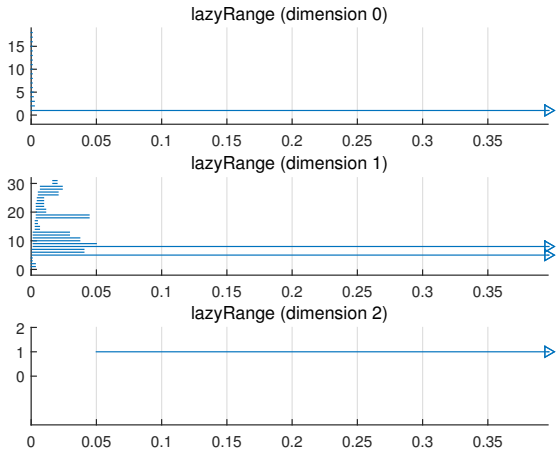

Figure 11: Barcodes for $K^6(200)$.

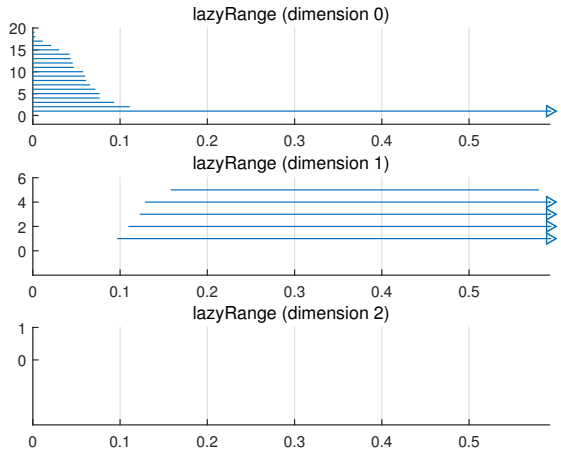

Figure 12: Barcodes for $CC_3^4(400)$.

6. Results for M_4 and M_6

To detect subspaces of M_4 whose topology is that of C_3, for any point $p \in C_3^3(400)$, we collect the points of M_4 that is the closest point to p (in Euclidean distance), written as $CC_3^4(400)$. One sample PLEX Betti barcode plot for $CC_3^4(400)$ is shown in Figure 12, which gives that $CC_3^4(400)$ has Betti numbers $\beta_0 = 1$ and $\beta_1 = 5$, i.e. having the topology of C_3. Similarly, we get one barcode plot result for the space $CC_3^6(400)$ in Figure 13, the result gives $\beta_0 = 1$ and $\beta_1 = 5$ in very small range of ϵ (from 0.26 to 0.31).

Remark 6.1. The Betti barcode result of space $CC_3^6(400)$ is not very stable, sometime it has not the homology of C_3. We ran 100 experiments on $CC_3^6(400)$, there only exist 69 experiments giving $\beta_0 = 1$, $\beta_1 = 5$.

As shown in above section, S^{31} and S^{71} have subspaces $K^4(200)$ and $K^6(200)$ with homology of a Klein bottle respectively. By using $K^4(200)$ and $K^6(200)$, subspaces of M_4 and M_6 are built, the method is as following.

We collect all the t closest points of M_4 to any $p \in K^4(200)$ (according to Euclidean distance) and denote it as $Kopt^4(200, t)$. The subspace $Kopt^6(200, t)$ of M_6 are constructed by the same way.

we consider the subspace $Kopt^4(200, 10)$, Figures 14, 15, 16 are three barcode results for $Kopt^4(200, 10)$. Figure 14 gives $\beta_0 = 1$, $\beta_1 = 2$ and $\beta_2 = 1$ from $\epsilon = 0.141$ to $\epsilon = 0.196$, Figure 15 indicates $\beta_0 = 1$, $\beta_1 = 2$

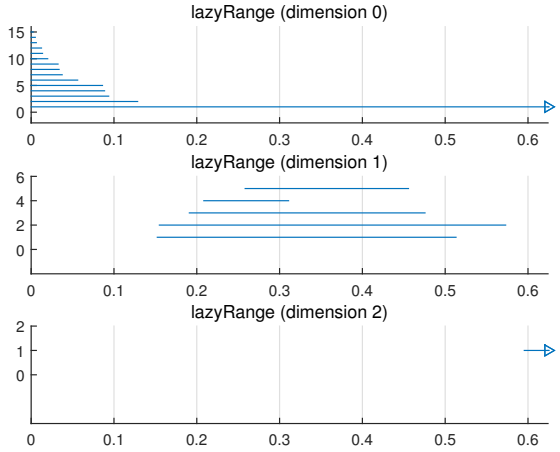

Figure 13: Barcodes for $CC_3^6(400)$.

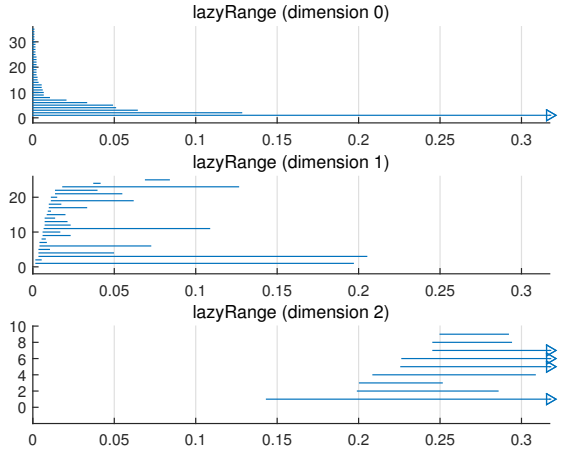

Figure 14: Barcodes for $Kopt^4(200, 10)$.

and $\beta_2 = 1$ in a very small range (only from $\epsilon = 0.195$ to $\epsilon = 0.206$), Figure 16 shows that there is no Klein bottle feature in $Kopt^4(200, 10)$.

Remark 6.2. We ran 300 trials on $Kopt^4(200, t)$ for $t = 10, 11, 12$, there are 92 experiments whose PLEX barcodes giving $\beta_0 = 1$, $\beta_1 = 2$ and $\beta_2 = 1$, the others have no homology of the Klein bottle. Hence we are not sure yet that $Kopt^4(200, 10)$ has Klein bottle feature, a further study need to be done.

Figures 17, 18 display two PLEX results for $Kopt^6(200, 10)$. In Figure 17, the PLEX barcode indicates $\beta_0 = 1$, $\beta_1 = 2$ and $\beta_2 = 1$ from 0.123 to 0.16. But in Figure 18, the PLEX barcode has no Klein bottle feature in $Kopt^6(200, 10)$. We ran 400 trials on $Kopt^6(200, t)$ for $t = 10, 11, 12$, there are 118 experiments whose PLEX barcodes giving $\beta_0 = 1$, $\beta_1 = 2$ and $\beta_2 = 1$ and some barcode intervals with $\beta_0 = 1$, $\beta_1 = 2$ and $\beta_2 = 1$ are very short, but the others have no homology of the Klein bottle.

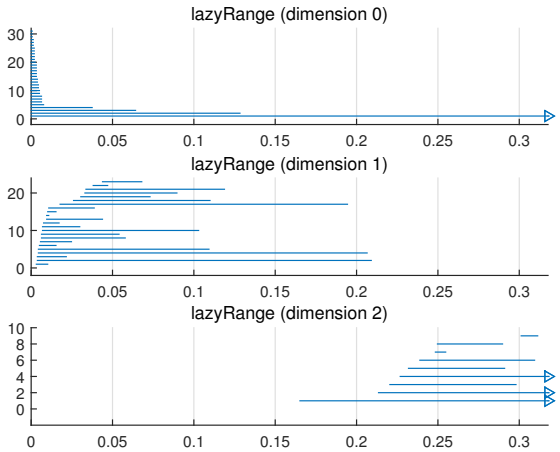

Figure 15: Barcodes for $Kopt^4(200, 10)$.

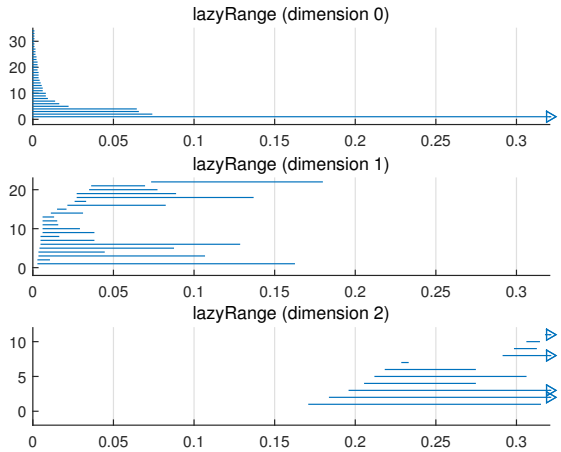

Figure 16: Barcodes for $Kopt^4(200, 10)$.

Remark 6.3. The authors of the paper [18] shown that there exist subspaces of spaces of 4×4 and 6×6 range image patches having the Klein bottle's homology, but when we use the same method to analyze 4×4 and 6×6 patches of optical flow, their Klein bottle feature are not obvious. Although the optical flow database are constructed from the range image database, spaces of 4×4 and 6×6 optical flow patches may have different topological characteristics as 4×4 and 6×6 range image patches.

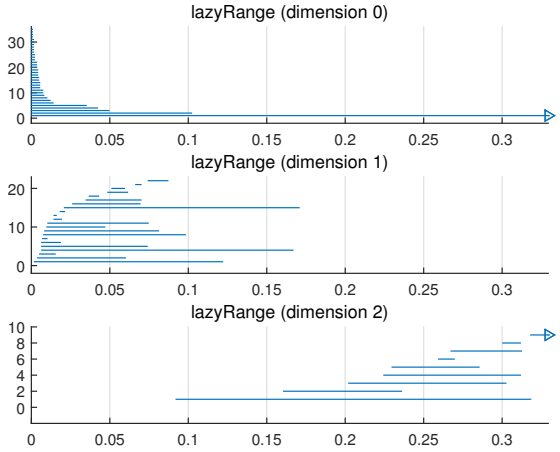

Figure 17: Barcodes for $Kopt^6(200, 10)$.

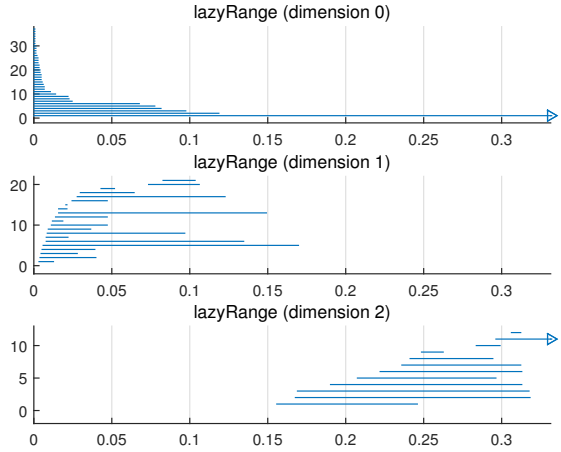

Figure 18: Barcodes for $Kopt^6(200, 10)$.

7. Conclusions

In this paper we study qualitative analysis of spaces of small optical flow patches by persistent homology. We show that the spaces of high contrast 4×4 and 6×6 patches have core subsets with the topology of a circle. The techniques used in this paper is not new, but we extend known results in the cases of 4×4 and 6×6 optical flow patches. Different sizes optical flow patches have similar properties, but they also have different features. By the current methods, we can not conclude that the spaces M_4 and M_6 have subspaces with homology of Klein bottle, perhaps they in fact have such subspaces, we seem to see their existence, so further investigation need to be done to determine whether M_4 and M_6 have subspaces with homology of the Klein bottle.

Acknowledgements

The author is very grateful to the referee for valuable comments and corrections. The project is supported by the National Natural Science Foundation of China (Grant No. 61471409).

References

[1] H. Adams, A. Atanasov, G. Carlsson, *Nudged elastic band in topological data analysis,* Topol. Methods Nonlinear Anal., **45** (2015), 247–272. 1, 4

[2] H. Adams, G. Carlsson, *On the nonlinear statistics of range image patches,* SIAM J. Image Sci., **2** (2009), 110–117. 1, 3, 4

[3] H. Adams, A. Tausz, *Javaplex tutorial,* http://javaplex.googlecode.com/svn/trunk/reports /javaplex tutorial/javaplex _tutorial.pdf. 2

[4] S. Baker, D. Scharstein, J. P. Lewis, S. Roth, M. J. Black, R. Szeliski, *A database and evaluation methodology for optical flow,* Int. J. Comput. Vision, **92** (2011), 1–31. 1

[5] J. L. Barron, D. J. Fleet, S. S. Beauchemin, *Performance of optical flow techniques,* Int. J. Comput. Vision, **12** (1994), 43–77. 1

[6] G. Carlsson, *Topology and data,* Bull. Amer. Math. Soc., **46** (2009), 255–308. 2

[7] G. Carlsson, T. Ishkhanov, V. de Silva, A. Zomorodian, *On the local behavior of spaces of natural images,* Int. J. Comput. Vision, **76** (2008), 1–12. 1, 3, 5, 5

[8] H. Edelsbrunner, D. Letscher, A. Zomorodian, *Topological persistence and simplification*, Discrete Comput. Geom., **28** (2002), 511–533. 2

[9] A. Geiger, P. Lenz, R. Urtasun, *Are we ready for autonomous driving? the kitti vision benchmark suite,* Computer Vision and Pattern Recognition (CVPR), 2012 IEEE Conference on IEEE, (2012). 1

[10] J. J. Gibson, *The senses considered as perceptual systems,* Houghton-Mifflin, Boston, (1966). 1

[11] K. Jia, X. Wang, X. Tang, *Optical flow estimation using learned sparse model,* IEEE International Conference on Computer Vision, November, (2011), 2391–2398. 1

[12] A. B. Lee, K. S. Pedersen, D. Mumford, *The nonlinear statistics of high-contrast patches in natural images,* Int. J. Comput. Vision, **54** (2003), 83–103. 3
[13] S. Roth, M. J. Black, *On the spatial statistics of optical flow,* Int. J. Comput. Vision, **74** (2007), 33–50. 1, 3
[14] V. d. Silva, G. Carlsson, *Topological estimation using witness complexes,* Proc. Sympos. Point-Based Graphics, (2004), 157–166. 2
[15] D. Sun, S. Roth, M. J. Black, *A quantitative analysis of current practices in optical flow estimation and the principles behind them,* Int. J. Comput. Vision, **106** (2014), 115–137. 1
[16] S. Xia, *On the local behavior of spaces of range image patches,* (To appear). 1, 4
[17] S. Xia , Y. Yin, *On the nonlinear analysis of optical flow,* (Submitted). 1, 4
[18] Q. Yin, W. Wang, *An analysis of spaces of range image small patches,* Open Cybern Syst. J., **9** (2015), 275–279. 1, 6.3
[19] A. Zomorodian, G. Carlsson, *Computing persistent homology,* Discrete Comput. Geom., **33** (2005), 249–274. 2